# Hydrodynamics beyond Navier-Stokes: The slip flow model

Wahyu P. Yudistiawan,[1] Santosh Ansumali,[1,*] and Iliya V. Karlin[2,3,†]
[1]*School of Chemical and Biomedical Engineering, Nanyang Technological University, 639798 Singapore*
[2]*Aerothermochemistry and Combustion Systems Lab, ETH Zurich, 8092 Zurich, Switzerland*
[3]*School of Engineering Sciences, University of Southampton, SO17 1BJ Southampton, United Kingdom*
(Received 11 February 2008; revised manuscript received 6 May 2008; published 24 July 2008)

Recently, analytical solutions for the nonlinear Couette flow demonstrated the relevance of the lattice Boltzmann (LB) models to hydrodynamics beyond the continuum limit [S. Ansumali *et al.*, Phys. Rev. Lett. **98**, 124502 (2007)]. In this paper, we present a systematic study of the simplest LB kinetic equation—the nine-bit model in two dimensions—in order to quantify it as a slip flow approximation. Details of the aforementioned analytical solution are presented, and results are extended to include a general shear- and force-driven unidirectional flow in confined geometry. Exact solutions for the velocity, as well as for pertinent higher-order moments of the distribution functions, are obtained in both Couette and Poiseuille steady-state flows for all values of rarefaction parameter (Knudsen number). Results are compared with the slip flow solution by Cercignani, and a good quantitative agreement is found for both flow situations. Thus, the standard nine-bit LB model is characterized as a valid and self-consistent slip flow model for simulations beyond the Navier-Stokes approximation.

DOI: 10.1103/PhysRevE.78.016705 PACS number(s): 47.11.−j, 05.70.Ln

## I. INTRODUCTION

The emerging field of fluid dynamics at a micrometer scale has become increasingly important due to fundamental engineering issues of micro-electromechanical systems [1]. Recently, much attention was given to the use of lattice Boltzmann (LB) models for simulation of microflows by a number of groups [2–8]. By now, it is understood that lattice Boltzmann models form a well-defined hierarchy based on discrete velocity sets with velocities defined as zeros of Hermite polynomials [9] or rational-number approximations thereof [10]. The LB hierarchy constitutes a novel approximation of the Boltzmann equation and has to be considered as an alternative to more standard approaches such as higher-order hydrodynamics (Burnett or super-Burnett) or Grad's moment systems (for a review, see, e.g., [11]). One salient feature of the LB hierarchy, which is crucial to the present study and eventually to any realistic application, is that it is naturally equipped with relevant boundary conditions derived from Maxwell-Boltzmann theory [2].

Agreement between the LB simulations and kinetic theory [2], hydrodynamics with slip boundary conditions [7], and molecular dynamics [8] was reported. However, most of these numerical works rely on simulation with finite accuracy, while the crucial question of whether the kinetic equations underpinning the LBM method are valid physical models of microflow remains unanswered. Thus, the validity of LBM cannot be addressed unless a comparison to representative exact solutions is performed. Needless to say, exact solutions to nonlinear kinetic equations in realistic geometries are very rare.

In a recent Letter [12], two of the present authors established an analytical approach to the lattice Boltzmann hierarchy of models, and found solutions for the first two models, namely the standard 9-bit model and the 16-bit model in the stationary nonlinear Couette flow in two dimensions. The solution demonstrated that, while the standard LB model amounts to a slip velocity approximation, the next members of the LB hierarchy do describe physically relevant Knudsen layers in the velocity profile. Thus, the LB hierarchy may provide a different—and computationally advantageous—approach to the physical phenomena in rarefied gases.

In this paper, we extend the results of Ref. [12] for the standard LB model. Specifically, we provide details of the exact solution of the D2Q9 LB model for the flow between parallel shearing plates (Couette flow), and we extend this solution to the presence of a forcing term in the kinetic equation, which mimics a flow driven by a pressure drop (Poiseuille flow). We use these solutions in order to quantify the accuracy of the standard LB model as a slip flow model. This quantification is usually done by defining a slip boundary condition in such a way that the velocity profile obtained from the Navier-Stokes equations with a slip boundary condition matches that obtained from a solution of kinetic equations for Poiseuille flow (see, for example, [13]). Specifically, in this formulation, for the slip boundary condition we have

$$u_{\mathrm{slip}}|_{\mathrm{wall}} = A_1 \mathrm{Kn}\left(\frac{\partial u_x}{\partial \hat{n}}\right)_{\mathrm{wall}} - A_2 \mathrm{Kn}^2\left(\frac{\partial^2 u_x}{\partial \hat{n}^2}\right)_{\mathrm{wall}}, \qquad (1)$$

where Kn is the Knudsen number [ratio of mean free path to the width of the slab; a more precise definition is given below, see Eq. (55)], the derivative of the velocity is taken in the direction of the inner normal to the wall, and where coefficients $A_1$ and $A_2$ are found by using the velocity profile obtained from a solution (exact or approximate) of the Boltzmann equation. These coefficients provide a convenient way to compare the accuracy of different approximations to the Boltzmann equation as many experimentally relevant

*ansumali@gmail.com
†Corresponding author. karlin.ilya@gmail.com

 

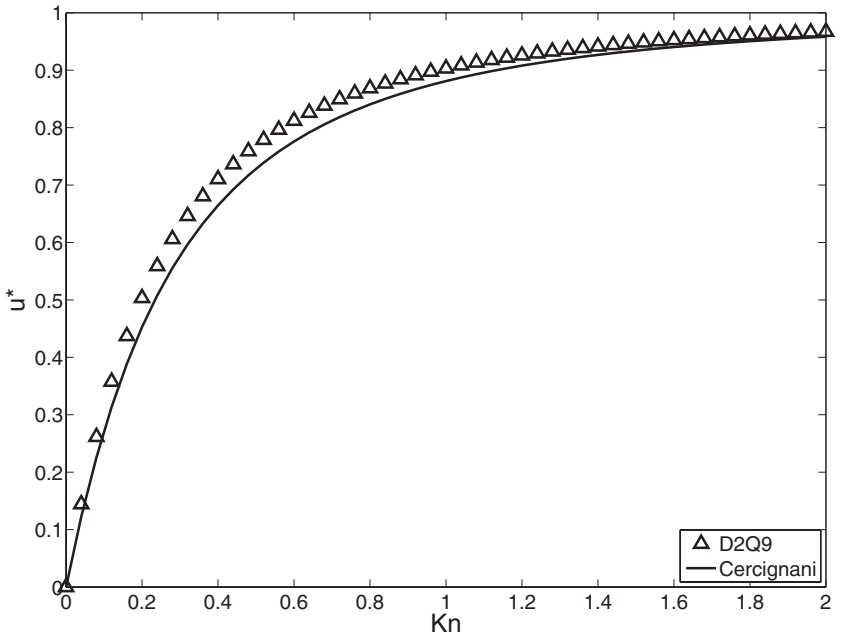


FIG. 1. Slip velocity versus Knudsen numbers for the Poiseuille flow.

quantities depend directly on these two coefficients. For example, in the Poiseuille flow, the minimum in the flow rate is observed at

$$\frac{1}{\mathrm{Kn}_{\min}} = 2\sqrt{3A_2}, \tag{2}$$

and the reduced slip velocity at the wall $u^*$ is

$$u^* = \frac{u_{\mathrm{slip}}}{u_{\mathrm{centerline}}} = \frac{A_1\mathrm{Kn} + 2A_2\mathrm{Kn}^2}{\frac{1}{4} + A_1\mathrm{Kn} + 2A_2\mathrm{Kn}^2}, \tag{3}$$

where $u_{\mathrm{slip}}$ is the slip velocity at the wall and $u_{\mathrm{centerline}}$ is the Poiseuille flow velocity at the centerline (i.e., the maximum) at a given Kn. We show in the present work that

$$A_1 = 1, \quad A_2 = \frac{2}{3} \tag{4}$$

for the lattice Boltzmann model with nine velocities. These values can be compared with the available approximate solution of the Boltzmann-Bhatnagar-Gross-Krook (BGK) equation by Cercignani, which gives

$$A_1 = 0.8297, \quad A_2 = 0.5108. \tag{5}$$

In Fig. 1, we compare the slip velocity obtained from an exact solution of the LB model with that obtained from an approximate solution of the Boltzmann-BGK equation. Similarly, in Fig. 2, we compare the flow rate as a function of Knudsen number for these two approaches. From these two plots, we see that the basic model of the LB hierarchy, the

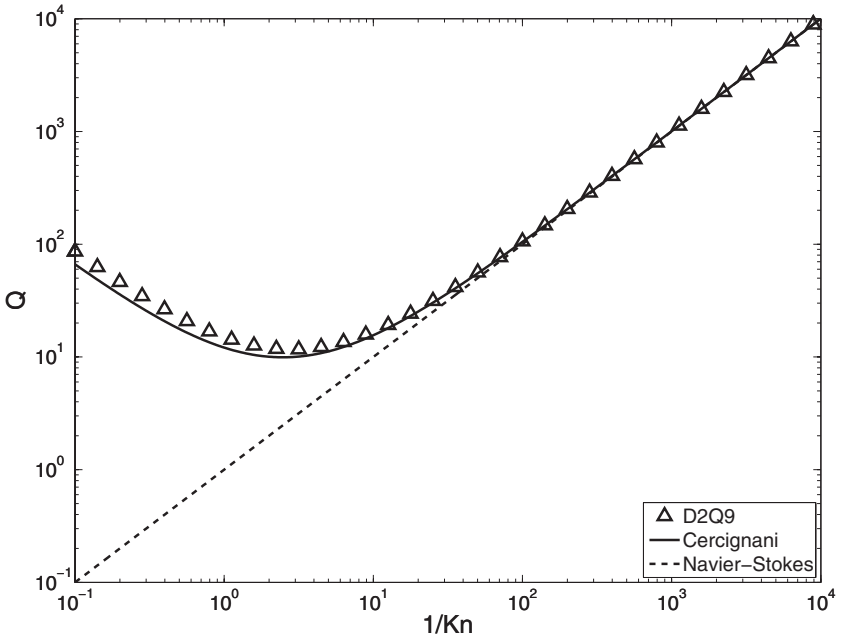


FIG. 2. Flowrate versus reciprocal of Knudsen number in log-log scale. The flowrate $Q$ is normalized such that $Q_{\mathrm{NS}} = \frac{1}{\mathrm{Kn}}$.

nonlinear D2Q9 model, can be quantified as the slip flow model for microflows.

The outline of the paper is as follows. In Sec. II, we recall the kinetic equation pertinent to the LB model with nine discrete velocities in two spatial dimensions, the D2Q9 model. We consider a general case that also includes a force term, and two popular forms of the force are presented. In Sec. III, we cast the kinetic equation in the form of a moment system for nine moments. The choice of the convenient moment representation proves important in the course of finding the solution. In Sec. IV, after describing the setup in which the fluid is confined between parallel moving plates, and is subject to the external force directed collinearly with the plates, we outline the strategy of finding the solution to the kinetic equation in the steady-state case. This strategy was already introduced in [12]. In the remainder of Sec. IV, we implement the solution strategy for the D2Q9 model: In Sec. IV B, we find the inner solution to the stationary moment system of Sec. III, assuming unidirectional flow and no mass flux through the walls. The solution is a parametric family depending on a set of constants of integration, which are later evaluated by applying specified boundary conditions. In Sec. IV C, we invert the map from the populations into the moments, and represent the populations as the functions of moments. This auxiliary step is required in order to impose the boundary conditions at the walls. In Sec. IV D, we apply the classical diffusive wall boundary conditions at the moving plates, and use the results of Secs. III and IV C in order to evaluate the integration constants of the moment solution. This is done in two steps: In Sec. IV D, a part of the integration constants is evaluated that enables us to write the solution in an explicit form for the velocity of the flow and for the off-diagonal (shear) stress, as a function of the Knudsen number. Evaluation of the remaining integration constants and finding the solution for rest of the higher-order moments is postponed until Sec. VI A. The explicit solutions of Sec. IV D are analyzed in Secs. V and V C, and compared with the slip flow solution by Cercignani from the linearized Boltzmann-BGK equation for the two limiting cases, Couette and Poiseuille flows. It is demonstrated in Sec. V that the solution for the nine-velocity model agrees quantitatively with the Boltzmann-BGK case. Another important access to the quality of a slip flow model is the behavior of the flow rate in the Poiseuille flow as a function of Knudsen number (so-called Knudsen minimum problem). In Sec. V C, the flow rate is compared to the result of Cercignani, and a good quantitative agreement is demonstrated. In Sec. VI A, we complete the solution by finding explicitly the higher-order moments. It is demonstrated that the normal stress difference shows a layer at the walls, and is in qualitative agreement with more microscopic simulations. In this section, we also investigate the question of the sensitivity of the results to the form of the forcing term in the discrete-velocity setting. Solution for a different choice of the forcing demonstrates that, while no changes occur in the basic fields (in particular in the velocity profile), the behavior of the higher-order nonhydrodynamic fields can be different. However, it is demonstrated that for slow flows (small Mach number) even this difference vanishes. Finally, a discussion is given in Sec. VII.

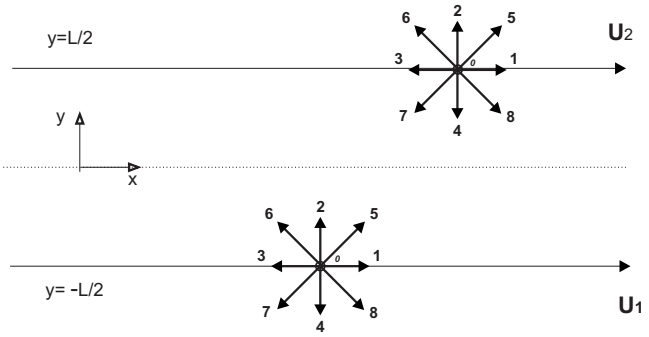


FIG. 3. Channel geometry. Discrete velocities of the D2Q9 model at the bottom and the top plates are indicated to explain boundary conditions.

## II. THE D2Q9 MODEL

The discrete velocity set for the D2Q9 model (see Fig. 3) is given by

$$c_x = \sqrt{\frac{3k_BT_0}{m}}\{0,1,0,-1,0,1,-1,-1,1\},$$

$$c_y = \sqrt{\frac{3k_BT_0}{m}}\{0,0,1,0,-1,1,1,-1,-1\}, \tag{6}$$

where $T_0$ is the reference temperature, $k_B$ is the Boltzmann constant, and $m$ is the molecular mass. Hereafter, $c_{ix}$ and $c_{iy}$ (the $i$th component of $c_x$ and $c_y$) will represent the $i$th component of discrete velocity vector $\mathbf{c}_i \equiv (c_{ix}, c_{iy})$. The distribution function $f$ (populations of the velocities $\mathbf{c}_i$, $i=0,\ldots,8$) will be represented by a vector,

$$f = \{f_0, f_1, f_2, f_3, f_4, f_5, f_6, f_7, f_8\}. \tag{7}$$

The entropy function of the D2Q9 model reads [14]

$$H = \sum_{i=0}^{8} f_i \ln\left(\frac{f_i}{w_i}\right), \tag{8}$$

where the vector of weights $w_i$ is

$$w = \frac{1}{36}\{16,4,4,4,4,1,1,1,1\}. \tag{9}$$

The local equilibrium distribution function, $f^{\mathrm{eq}}$, is found upon minimizing $H$ (8), subject to fixed density $\rho$ and momentum $j_\alpha$, $\alpha = x, y$,

$$\rho(f) = \sum_{i=0}^{8} f_i,$$

$$j_\alpha(f) = \sum_{i=0}^{8} c_{i\alpha} f_i. \tag{10}$$

The result of this minimization problem reads [9]

$$f_i^{\mathrm{eq}} = \rho w_i \prod_{\alpha=1}^{D} \left[ \left( \frac{2c - \sqrt{3u_\alpha^2 + c^2}}{c} \right) \left( \frac{2u_\alpha + \sqrt{3u_\alpha^2 + c^2}}{c - u_\alpha} \right)^{c_{i\alpha}/c} \right]. \tag{11}$$

Here $c = \sqrt{3} c_s$, where $c_s$ is the speed of sound,

$$c_s = \sqrt{\frac{k_B T_0}{m}}, \tag{12}$$

with $T_0$ the reference temperature and $m$ the mass of a particle. The fluid velocity $u_\alpha$ is defined as

$$u_\alpha = \frac{j_\alpha}{\rho}, \tag{13}$$

and $D=2$ in the present case. Expanding Eq. (11) into powers of velocity to second order, we obtain the series expansion of the equilibrium [15] which will be used throughout the paper,

$$f_i^{\mathrm{eq}} = w_i \left[ \rho + \frac{j_\alpha c_{i\alpha}}{c_s^2} + \frac{j_\alpha j_\beta}{2\rho c_s^4} (c_{i\alpha} c_{i\beta} - c_s^2 \delta_{\alpha\beta}) \right]. \tag{14}$$

Using the BGK collision model and applying a force term, the kinetic equation for the populations $f_i$ can be written as

$$\partial_t f_i + c_{i\alpha} \partial_\alpha f_i - \mathcal{F}_i = -\frac{1}{\tau} (f_i - f_i^{\mathrm{eq}}), \tag{15}$$

where $\mathbf{g} \equiv \{g_x, g_y\}$ is the acceleration vector and $\tau$ is the relaxation time, which relates to the kinematic viscosity $\nu$ through

$$\nu = \tau c_s^2. \tag{16}$$

A remark on the choice of the forcing term in the kinetic equation (15) is in order. In the discrete-velocity case, we do not have derivatives in the velocities, thus the familiar forcing term of the classical kinetic theory, viz., $g_\alpha (\partial f / \partial c_\alpha)$, is not applicable. In general, any forcing term is a valid approximation as long as its lower-order moments coincide with the moments of $g_\alpha (\partial f / \partial c_\alpha)$ with at least second-order accuracy. For example, the forcing term [16]

$$\mathcal{F}_i^{(1)} = g_\alpha \frac{(c_{i\alpha} - u_\alpha)}{c_s^2} f_i^{\mathrm{eq}} \tag{17}$$

is often used in the simulation due to its compact form. An alternate form of the force is also used in the literature [17]

$$\mathcal{F}_i^{(2)} = w_i \rho \left( \frac{g_\alpha c_{i\alpha}}{c_s^2} + \frac{g_\beta j_\alpha + g_\alpha j_\beta}{2\rho c_s^4} (c_{i\alpha} c_{i\beta} - c_s^2 \delta_{\alpha\beta}) \right). \tag{18}$$

One of the objectives of this paper is to analyze the effect of the choice of the forcing.

## III. MOMENT REPRESENTATION

In a sequel, we shall also need a different but equivalent representation of the kinetic equation (15) in terms of nine linearly independent linear combinations of the populations (moments). The three locally conserved moments (density and two components of the momentum density) have already been introduced above [see Eq. (10)]. The remaining six independent moments are most conveniently chosen as follows:

Three independent components of the pressure tensor,

$$P_{\alpha\beta}(f) = \sum_{i=0}^{8} f_i c_{i\alpha} c_{i\beta},$$

which we choose as the diagonal elements, $P_{xx}$ and $P_{yy}$, and the off-diagonal (shear) component, $P_{xy}$; two independent components, $Q_{xyy}$ and $Q_{yxx}$, of the third-order moment tensor,

$$Q_{\alpha\beta\gamma}(f) = \sum_{i=0}^{8} f_i c_{\alpha i} c_{i\beta} c_{i\gamma},$$

and a fourth-order moment, $R_{xxyy}$, where

$$R_{\alpha\beta\gamma\theta}(f) = \sum_{i=0}^{8} f_i c_{i\alpha} c_{i\beta} c_{i\gamma} c_{i\theta}.$$

Note that a different choice of the moments was used in Ref. [12]. By the equivalence of bases theorem, any other choice of the basis in the nine-dimensional state space of the present model is possible and was used in previous works [18]. For our present purpose, the above choice of the moment system proves to be most convenient. The set of nine moments just introduced is represented by a nine-dimensional vector $\mathcal{M}(f)$,

$$\mathcal{M} = \{\rho, j_x, j_y, P_{xx}, P_{xy}, P_{yy}, Q_{yxx}, Q_{xyy}, R_{xxyy}\}, \tag{19}$$

which is compactly represented by a relation (from populations to moments)

$$\mathcal{M} = \Psi \cdot f, \tag{20}$$

where $\Psi$ is a $9 \times 9$ matrix,

$$\Psi = \{1, c_x, c_y, c_x c_x, c_x c_y, c_y c_y, c_x c_x c_y, c_x c_y c_y, c_x c_x c_y c_y\}, \tag{21}$$

with $1 = \{1,1,1,1,1,1,1,1,1\}$. Any other moment can be expressed as a linear combinations of the set $\mathcal{M}$. It is easy to check using Eq. (14) that at the equilibrium, $\mathcal{M}^{\mathrm{eq}} = \mathcal{M}(f^{\mathrm{eq}}(\rho, \mathbf{j}))$, where

$$\mathcal{M}^{\mathrm{eq}} = \left\{ \rho, j_x, j_y, \frac{j_x^2}{\rho} + \rho c_s^2, \frac{j_x j_y}{\rho}, \frac{j_y^2}{\rho} + \rho c_s^2, j_y c_s^2, j_x c_s^2, \frac{j^2}{\rho} c_s^2 + \rho c_s^4 \right\}. \tag{22}$$

Elsewhere below, the nonequilibrium value of any moment, $\mathcal{M} - \mathcal{M}^{\mathrm{eq}}$, will be denoted as $\mathcal{M}^{\mathrm{neq}}$. Furthermore, the moments of any valid forcing vector $\mathcal{F}$ are of the form

$$\mathcal{M}(\mathcal{F}) = \{0, \rho g_x, \rho g_y, \phi_1(\mathcal{F}), \phi_2(\mathcal{F}), \phi_3(\mathcal{F}), \phi_4(\mathcal{F}), \phi_5(\mathcal{F}), \phi_6(\mathcal{F})\}. \tag{23}$$

For the two types of forcing considered here, Eqs. (17) and (18), the moments are provided in Appendix D.

Applying Eq. (20) to Eq. (15), we obtain the time evolution equations for the moments. Specifically, for the locally conserved fields, we have

$$\partial_t \rho + \partial_x j_x + \partial_y j_y = 0,$$

$$\partial_t j_x + \partial_x P_{xx} + \partial_y P_{xy} - \rho g_x = 0,$$

$$\partial_t j_y + \partial_x P_{xy} + \partial_y P_{yy} - \rho g_y = 0. \tag{24}$$

For the components of the pressure tensor, we have

$$\partial_t P_{xx} + 3c_s^2 \partial_x j_x + \partial_y Q_{yxx} - \phi_1 = -\frac{1}{\tau}\left(P_{xx} - \frac{j_x^2}{\rho} - \rho c_s^2\right),$$

$$\partial_t P_{xy} + \partial_x Q_{yxx} + \partial_y Q_{xyy} - \phi_2 = -\frac{1}{\tau}\left(P_{xy} - \frac{j_x j_y}{\rho}\right),$$

$$\partial_t P_{yy} + \partial_x Q_{xyy} + 3c_s^2 \partial_y j_y - \phi_3 = -\frac{1}{\tau}\left(P_{yy} - \frac{j_y^2}{\rho} - \rho c_s^2\right). \tag{25}$$

Finally, for the rest of the higher-order moments, we have

$$\partial_t Q_{yxx} + 3c_s^2 \partial_x P_{xy} + \partial_y R_{xxyy} - \phi_4 = -\frac{1}{\tau}\left(Q_{yxx} - j_y c_s^2\right),$$

$$\partial_t Q_{xyy} + \partial_x R_{xxyy} + 3c_s^2 \partial_y P_{xy} - \phi_5 = -\frac{1}{\tau}\left(Q_{xyy} - j_x c_s^2\right),$$

$$\partial_t R_{xxyy} + 3c_s^2 \partial_x Q_{xyy} + 3c_s^2 \partial_y Q_{yxx} - \phi_6 = -\frac{1}{\tau}\left(R_{xxyy} - \frac{j^2}{\rho} c_s^2 - \rho c_s^4\right). \tag{26}$$

The moment system (24)–(26) for nine moments is equivalent to the kinetic equation. In the course of finding the solution to a generalized unidirectional flow (see next section), both the moment and the population representations will be used.

## IV. UNIDIRECTIONAL FLOW: STATIONARY SOLUTION

### A. Setup description and outline of solution

We consider the fluid to be enclosed by two parallel plates in the $x$ direction and separated by a distance of $L$ (see Fig. 3). The bottom plate at $y=-L/2$ moves with the velocity $U_1$ and the top plate at $y=L/2$ moves with the velocity $U_2$. Unidirectional forcing in the $x$ direction is also added ($\mathbf{g}=\{g,0\}$). We aim at finding the steady-state solution to the kinetic equation of Sec. II (or, equivalently, of the moment system of Sec. III) in this setup.

Let us outline the solution strategy, which consists of three steps:

*Step 1.* Integration of the steady-state moment system. This is done under two assumptions: (i) The flow is unidirectional. All the fields depend only on the $y$ coordinate. (ii) No mass flow through the walls. As a result, we find the inner solution for all the moments. This inner solution is a parametric family that depends on four yet undetermined constants of integration.

*Step 2.* Inner solution for the populations. In this step, we invert the map from the population space to the moments space, and use a representation of the populations in terms of moments. This representation is similar to Grad's distribution function, albeit in the present context it is exact representation. Using the result of step 1, we find the inner solution for the populations. The latter depends on the same integration constants as introduced above. This step is required in order to apply the boundary conditions at the next step.

*Step 3.* Matching the boundary condition for the populations with the inner solution. Accordingly, we apply the diffusively reflecting wall boundary condition at the top and bottom plates and match it with the inner solution for the populations. Thereby, the integration constants will be unambiguously determined, and the solution for the moments can be found. The complete solution for the Couette and Poiseuille flow setup will be explicitly given. Note that in this part, solving for $j_x$ is prioritized and some related moments are solved as well. A separate section is dedicated to discussing the remaining moments.

### B. Step 1. Inner solution to the stationary moment system

Assuming that the flow is in the steady state and is unidirectional (all the fields depend only of the $y$ coordinate due to the nature of the setup, which is infinite in the $x$ direction), the stationary moment system reads (with some rearrangement of the order of the equations that will prove useful below)

$$\partial_y j_y = 0, \tag{27}$$

$$\partial_y P_{yy} = 0,$$

$$3c_s^2 \partial_y j_y - \phi_3 = -\frac{1}{\tau}\left(P_{yy} - \frac{j_y^2}{\rho} - \rho c_s^2\right), \tag{28}$$

$$\partial_y P_{xy} - \rho g = 0,$$

$$\partial_y Q_{xyy} - \phi_2 = -\frac{1}{\tau}\left(P_{xy} - \frac{j_x j_y}{\rho}\right),$$

$$3c_s^2 \partial_y P_{xy} - \phi_5 = -\frac{1}{\tau}(Q_{xyy} - j_x c_s^2), \tag{29}$$

$$\partial_y Q_{yxx} - \phi_1 = -\frac{1}{\tau}\left(P_{xx} - \frac{j_x^2}{\rho} - \rho c_s^2\right),$$

$$\partial_y R_{xxyy} - \phi_4 = -\frac{1}{\tau}\left(Q_{yxx} - j_y c_s^2\right),$$

$$3c_s^2\partial_y Q_{yxx} - \phi_6 = -\frac{1}{\tau}\left(R_{xxyy} - \frac{j_x^2 + j_y^2}{\rho}c_s^2 - \rho c_s^4\right). \quad (30)$$

From Eq. (27) and the no-flux condition at the walls, $j_y|_{\text{wall}} = 0$, we obtain that the transverse momentum flux is vanishing,

$$j_y = 0. \quad (31)$$

Substituting $j_y = 0$ into the rest of the moment equations, we arrive at three decoupled sets of equations. Using Eqs. (D1) and (D2), we see that for both types of forcing, we have

$$\phi_2 = \phi_3 = \phi_4 = 0, \quad \phi_5 = \rho c_s^2 g. \quad (32)$$

Let us now integrate the resulting moment system. From the first set (28), we find

$$P_{yy} = \rho c_s^2,$$

$$\rho = \text{const}, \quad (33)$$

that is, the density is a constant. From the second set (29), we find

$$P_{xy}(y) = \rho g y + k_1,$$

$$Q_{xyy}(y) = c_s^2[j_x(y) - 2\rho g \tau],$$

$$j_x(y) = -\frac{\rho g}{2\tau c_s^2}y^2 - \frac{k_1}{\tau c_s^2}y + \left(\frac{k_2}{c_s^2} + 2\rho g \tau\right), \quad (34)$$

where $k_1$ and $k_2$ are yet undetermined constants of integration. This result shows that the macroscopic velocity profile is insensitive to the choice of the particular form of the forcing.

Finally, the third set (30) can be simplified in terms of two auxiliary functions,

$$X_1 = R_{xxyy}^{\text{neq}} + \sqrt{3}c_s Q_{yxx}^{\text{neq}},$$

$$X_2 = R_{xxyy}^{\text{neq}} - \sqrt{3}c_s Q_{yxx}^{\text{neq}}. \quad (35)$$

The nonequilibrium part of the normal stress can be written as follows:

$$\mathcal{N}^{\text{neq}} = \frac{X_1 + X_2}{6c_s^2} - \frac{\tau}{3c_s^2}(\phi_6 - 3c_s^2\phi_1), \quad (36)$$

while $X_1$ and $X_2$ satisfy

$$\partial_y\left\{X_1 \exp\left(\frac{y}{\tau\sqrt{3}c_s}\right)\right\} = \exp\left(\frac{y}{\tau\sqrt{3}c_s}\right)\left\{\frac{\phi_6}{\sqrt{3}c_s} - \partial_y R_{xxyy}^{\text{eq}}\right\},$$

$$\partial_y\left\{X_2 \exp\left(-\frac{y}{\tau\sqrt{3}c_s}\right)\right\} = -\exp\left(-\frac{y}{\tau\sqrt{3}c_s}\right)\left\{\frac{\phi_6}{\sqrt{3}c_s} + \partial_y R_{xxyy}^{\text{eq}}\right\}, \quad (37)$$

which, upon integration, gives

$$X_1(y) = X_1(y_1)\exp\left(\frac{(y_1 - y)}{\tau\sqrt{3}c_s}\right) + \int_{s=y_1}^{s=y} ds \exp\left(\frac{s - y}{\tau\sqrt{3}c_s}\right) \times\left\{\frac{\phi_6[j_x(s)]}{\sqrt{3}c_s} + \frac{2}{\tau}u_x(s)P_{xy}(s)\right\},$$

$$X_2(y) = X_2(y_2)\exp\left(\frac{-(y_2 - y)}{\tau\sqrt{3}c_s}\right) - \int_{s=y_2}^{s=y} ds \exp\left(\frac{(y - s)}{\tau\sqrt{3}c_s}\right) \times\left\{\frac{\phi_6[j_x(s)]}{\sqrt{3}c_s} - \frac{2}{\tau}u_x(s)P_{xy}(s)\right\}. \quad (38)$$

Here $y_1$ and $y_2$ are two fixed points, at which the values of $X_1$ and $X_2$ have to be provided, and we have used the fact that Eqs. (29) can be rewritten as

$$\partial_y j_x = -\frac{P_{xy}}{\tau c_s^2}. \quad (39)$$

Using integration by parts, Eq. (38) can be simplified as

$$X_1(y) = \exp\left(\frac{y_1 - y}{\tau\sqrt{3}c_s}\right)\{X_1(y_1) - \Theta_1(y_1)\} + \Theta_1(y),$$

$$X_2(y) = \exp\left(-\frac{y_2 - y}{\tau\sqrt{3}c_s}\right)\{X_2(y_2) - \Theta_2(y_2)\} + \Theta_2(y), \quad (40)$$

where

$$\Theta_1 = \frac{6}{\rho}P_{xy}^2 + (2u_x - 18\tau g)(\sqrt{3}c_s P_{xy} - 3\tau c_s^2\rho g) + \tau\phi_6 - \sqrt{3}\tau^2 c_s\partial_y\phi_6 + 3\tau^3 c_s^2\partial_y^2\phi_6 - 3\sqrt{3}\tau^4 c_s^3\partial_y^3\phi_6 + 9\tau^5 c_s^4\partial_y^4\phi_6 - 9\sqrt{3}\tau^6 c_s^5\partial_y^5\phi_6 + 27\tau^7 c_s^6\partial_y^6\phi_6,$$

$$\Theta_2 = \frac{6}{\rho}P_{xy}^2 - (2u_x - 18\tau g)(\sqrt{3}c_s P_{xy} + 3\tau c_s^2\rho g) + \tau\phi_6 + \sqrt{3}\tau^2 c_s\partial_y\phi_6 + 3\tau^3 c_s^2\partial_y^2\phi_6 + 3\sqrt{3}\tau^4 c_s^3\partial_y^3\phi_6 + 9\tau^5 c_s^4\partial_y^4\phi_6 + 9\sqrt{3}\tau^6 c_s^5\partial_y^5\phi_6 + 27\tau^7 c_s^6\partial_y^6\phi_6, \quad (41)$$

and we have used the fact that for both the forcing schemes under consideration, $\phi_6$ is at most a sixth-order polynomial in $y$ (that is, expressions for $\Theta_1$ and $\Theta_2$ are still exact).

In summary, Eqs. (31), (33), (34), (40), and (36) provide the general inner solution for the stationary moment system, and it depends on four parameters: two integration constants, $k_1, k_2$, and two values of $X_1$ and $X_2$ at some specified points, $y_1$ and $y_2$, respectively. To determine these, we need to specify boundary conditions at the walls. Note that this is precisely where the LB hierarchy differs from the method of moments. It is well known that for moment methods, such as Grad's systems, it is not possible to provide self-consistent boundary conditions for the moments. In our case, this is possible because the boundary conditions for the LB kinetic equations are formulated in terms of populations rather than in terms of moments. For that, we need to invert the linear relation between the moments and the populations, which is done in the next section.

### C. Step 2. Population representation of the inner solution

In this auxiliary section, we consider the following basis of the nine-dimensional space:

$$e = \{1, c_x, c_y, (c_x c_x - c_s^2 1), c_x c_y, (c_y c_y - c_s^2 1), (c_x c_x c_y - c_s^2 c_y), (c_x c_y c_y - c_s^2 c_x), (c_x c_x - c_s^2 1)(c_y c_y - c_s^2 1)\}. \tag{42}$$

The basis (42) is orthogonal with respect to the scalar product $\langle x,y\rangle = \Sigma_{i=0}^{8} w_i x_i y_i$. We represent the population vector $f$ in the basis (42),

$$f = \sum_{k=0}^{8} w_k e_k \varphi_k, \tag{43}$$

where expansion coefficients $\varphi_k$ are found by taking the inner product of $f$ with the basis elements $e_k$. Thus, the populations can be written in a Grad-like form (from-moments-to-populations representation),

$$f_i = w_i \left( \rho + \frac{j_\alpha c_{i\alpha}}{c_s^2} + \frac{\mathcal{G}_i^{(2)}}{2c_s^4} + \frac{\mathcal{G}_i^{(3)}}{6c_s^6} + \frac{\mathcal{G}_i^{(4)}}{4c_s^8} \right), \tag{44}$$

where

$$\mathcal{G}_i^{(2)} = (P_{\alpha\beta} - \rho c_s^2 \delta_{\alpha\beta})(c_{i\alpha} c_{i\beta} - c_s^2 \delta_{\alpha\beta}),$$

$$\mathcal{G}_i^{(3)} = (Q_{\alpha\beta\gamma} - j_\alpha c_s^2 \delta_{\beta\gamma} - j_\beta c_s^2 \delta_{\alpha\gamma} - j_\gamma c_s^2 \delta_{\alpha\beta}) \times [c_{i\alpha} c_{i\beta} c_{i\gamma} - c_s^2 (c_{i\alpha}\delta_{\beta\gamma} + c_{i\beta}\delta_{\alpha\gamma} + c_{i\gamma}\delta_{\alpha\beta})],$$

$$\mathcal{G}_i^{(4)} = (R_{xxyy} - P c_s^2 + \rho c_s^4)(c_{ix}^2 - c_s^2)(c_{iy}^2 - c_s^2). \tag{45}$$

Note that $P = P_{\alpha\alpha} = P_{xx} + P_{yy}$. The explicit form of the individual populations $f_i$ can be found in Appendix A.

Upon substituting the solution for the moments obtained in Sec. IV B into Eqs. (44) and (45), we obtain the inner solution in terms of populations. Note that populations obtained in this way depend on the same four integration constants previously introduced. Thus, the result of this section enables us to impose the boundary conditions, which is done in the next section.

### D. Step 3. From boundary condition to explicit solution

#### 1. Diffusive wall boundary condition

Boundary conditions for discrete velocity models are formulated in terms of populations (distribution function). Thus, in order to apply the boundary conditions, it is convenient to come back from the moment representation to the representation in terms of the distribution using Eq. (44). For the present system, we apply the classical Maxwell's diffusive wall boundary condition. In this condition, particles that reach the wall are redistributed in a way consistent with the mass-balance and normal-flux conditions,

$$f_i\big|_{\mathbf{c}_i\cdot\mathbf{n}>0} = \frac{\sum_{\mathbf{c}_i\cdot\mathbf{n}<0} |(\mathbf{c}_i\cdot\mathbf{n})| f_i}{\sum_{\mathbf{c}_i\cdot\mathbf{n}<0} |(\mathbf{c}_i\cdot\mathbf{n})| f_i^{\mathrm{eq}}(\rho, \mathbf{U}_{\mathrm{wall}})} f_i^{\mathrm{eq}}(\rho, \mathbf{U}_{\mathrm{wall}}), \tag{46}$$

where $\mathbf{n}$ is the inner normal at the wall, and $\mathbf{U}_{\mathrm{wall}}$ is the wall velocity. Equation (46) means that the redistribution of the particles that reach the wall will be according to the equilibrium distribution of the population that leaves the wall. Note that the dependence on the density entering the wall equilibrium distribution $f_i^{\mathrm{eq}}(\rho, \mathbf{U}_{\mathrm{wall}})$ is immaterial in Eq. (46); it cancels out both in the numerator and the denominator because the density dependence factors out. In order to avoid confusion, we shall rewrite Eq. (46) using a nominal value $\rho = 1$,

$$f_i\big|_{\mathbf{c}_i\cdot\mathbf{n}>0} = \frac{\sum_{\mathbf{c}_i\cdot\mathbf{n}<0} |(\mathbf{c}_i\cdot\mathbf{n})| f_i}{\sum_{\mathbf{c}_i\cdot\mathbf{n}<0} |(\mathbf{c}_i\cdot\mathbf{n})| f_i^{\mathrm{eq}}(1, \mathbf{U}_{\mathrm{wall}})} f_i^{\mathrm{eq}}(1, \mathbf{U}_{\mathrm{wall}}). \tag{47}$$

Let us proceed with evaluating the left-hand side of Eq. (47) for the present case. First, using the formula for the equilibrium (14), and taking into account that $\mathbf{U}_{\mathrm{wall}} = \{U_{\mathrm{wall}}, 0\}$, where $U_{\mathrm{wall}} = U_1$ for the lower plate and $U_{\mathrm{wall}} = U_2$ the upper plate, we obtain the equilibrium of the populations leaving the walls,

$$f_i^{\mathrm{eq}}(1, U_{\mathrm{wall}}) = w_i \left( 1 + \frac{c_{ix} U_{\mathrm{wall}}}{c_s^2} + \frac{(c_{ix} U_{\mathrm{wall}})^2}{2c_s^4} - \frac{U_{\mathrm{wall}}^2}{2c_s^2} \right). \tag{48}$$

Second, noticing that $|(\mathbf{c}_i\cdot\mathbf{n})| = c = \sqrt{3} c_s$ for all $i$ satisfying $\mathbf{c}_i\cdot\mathbf{n} < 0$, the denominator in Eq. (47) is evaluated using the equilibrium (48) and the auxiliary identities collected in Appendix B, Eq. (B1),

$$\sum_{\mathbf{c}_i\cdot\mathbf{n}<0} |(\mathbf{c}_i\cdot\mathbf{n})| f_i^{\mathrm{eq}}(1, U_{\mathrm{wall}}) = \frac{c}{6}. \tag{49}$$

Equation (49) is valid for both the top and the bottom plates since the identities in Eq. (B1) are the same for either case of $c_{iy} < 0$ or $c_{iy} > 0$. Third and final, using identities given in Appendix C, we evaluate the nominator in Eq. (47) (the total flux of impinging populations),

$$\sum_{\mathbf{c}_i\cdot\mathbf{n}<0} |(\mathbf{c}_i\cdot\mathbf{n})| f_i = c \sum_{\mathbf{c}_i\cdot\mathbf{n}<0} w_i \left( \rho + \frac{j_\alpha c_{i\alpha}}{c_s^2} + \frac{\mathcal{G}_i^{(2)}}{2c_s^4} + \frac{\mathcal{G}_i^{(3)}}{6c_s^6} + \frac{\mathcal{G}_i^{(4)}}{4c_s^8} \right) = \frac{c\rho}{6}. \tag{50}$$

Here $\rho$ is the density of the fluid found above (that is, $\rho = \mathrm{const}$).

Combining together the results (48)–(50), we find the diffusive wall boundary conditions in the present setup,

$$f_i\big|_{\mathbf{c}_i\cdot\mathbf{n}>0} = \rho f_i^{\mathrm{eq}}(1, U_{\mathrm{wall}}) = f_i^{\mathrm{eq}}(\rho, U_{\mathrm{wall}}). \tag{51}$$

Thus, in the present steady-state flow, the boundary condition amounts to setting the outgoing populations at the wall equi-

librium. For the purpose of what will follow, we shall write Eq. (51) for each individual population explicitly: At $y=-L/2$ (bottom wall),

$$f_2|_{y=-L/2} = \frac{4}{36}\rho\left(1 - \frac{1}{2c_s^2}U_1^2\right),$$

$$f_5|_{y=-L/2} = \frac{1}{36}\rho\left(1 + \frac{\sqrt{3}}{c_s}U_1 + \frac{1}{c_s^2}U_1^2\right),$$

$$f_6|_{y=-L/2} = \frac{1}{36}\rho\left(1 - \frac{\sqrt{3}}{c_s}U_1 + \frac{1}{c_s^2}U_1^2\right), \tag{52}$$

and at $y=L/2$ (top wall),

$$f_4|_{y=L/2} = \frac{4}{36}\rho\left(1 - \frac{1}{2c_s^2}U_2^2\right),$$

$$f_7|_{y=L/2} = \frac{1}{36}\rho\left(1 - \frac{\sqrt{3}}{c_s}U_2 + \frac{1}{c_s^2}U_2^2\right),$$

$$f_8|_{y=L/2} = \frac{1}{36}\rho\left(1 + \frac{\sqrt{3}}{c_s}U_2 + \frac{1}{c_s^2}U_2^2\right). \tag{53}$$

In the next section, we match the inner solution for the populations with the boundary condition.

#### 2. Evaluation of $k_1$ and $k_2$

In the first step of the matching procedure, we evaluate the two integration constants $k_1$ and $k_2$. This will be sufficient for finding the closed-form velocity profile and the shear stress, and thus to quantify the slip model. Functions $Q_{xyy}(y;k_1,k_2)$ and $P_{xy}(y;k_1,k_2)$ are given by the inner solution, Eq. (34). Substituting these into boundary condition Eq. (A4), we arrive at two linear algebraic equations for the two unknowns, $k_1$ and $k_2$. After some algebra, we find

$$k_1 = -\frac{\rho\nu}{(2\mathrm{Kn}+1)}\frac{(U_2-U_1)}{L},$$

$$k_2 = \rho c_s^2\frac{(U_1+U_2)}{2} + \frac{\rho c_s^2 g}{2\nu}(4\mathrm{Kn}+1)\left(\frac{L}{2}\right)^2. \tag{54}$$

Here we have introduced the Knudsen number,

$$\mathrm{Kn} = \frac{\sqrt{3}\tau c_s}{L}. \tag{55}$$

Note that mean free path $l_{\mathrm{m.f.p.}}$ is defined as

$$l_{\mathrm{m.f.p.}} = \sqrt{3}\tau c_s, \tag{56}$$

so that $\mathrm{Kn}=l_{\mathrm{m.f.p.}}/L$.

With Eq. (54), Eq. (34) give us closed-form expressions for the velocity profile, shear stress, and the $xyy$ component of the third-order moments tensor. This information is sufficient in order to compare the present D2Q9 model with other known results of kinetic theory. Therefore, we shall do this in the next section, and will complete the solution for the rest of the higher-order moments (which requires evaluation of the two remaining integration constants) in Sec. IV A.

## V. SLIP MODEL

### A. Velocity profile

Using Eq. (54) in Eq. (34), and with some rearrangement of the terms, we find the solution for the $x$ component of the velocity $u_x=j_x/\rho$,

$$u_x = \frac{gL^2}{2\nu}\left[-\left(\frac{y}{L}-\frac{1}{2}\right)\left(\frac{y}{L}+\frac{1}{2}\right) + \mathrm{Kn} + \frac{4}{3}\mathrm{Kn}^2\right] + \frac{(U_2-U_1)}{(2\mathrm{Kn}+1)}\frac{y}{L} + \frac{(U_1+U_2)}{2}, \tag{57}$$

while for the off-diagonal component of the pressure tensor, we have

$$P_{xy} = \rho g y - \frac{\rho\nu}{(2\mathrm{Kn}+1)}\frac{(U_2-U_1)}{L}. \tag{58}$$

It is instructive to consider the two limiting cases of the general expressions (57) and (58). For a purely shear driven flow (Couette flow), we set $g=0$. Then formulas (57) and (58) recover the solution already derived in our previous Letter [12]. On the other hand, in the case of Poiseuille flow, we set $U_1=U_2=U$ to obtain in Eq. (57) the familiar parabolic velocity profile with an additional slip correction terms of the order Kn and $\mathrm{Kn}^2$. The latter indicates that the D2Q9 model amounts to the second-order slip velocity model to be discussed in the next section.

### B. Second-order slip velocity

In order to characterize the D2Q9 as a slip velocity model, let us introduce the slip velocity at the walls,

$$u_{\mathrm{slip}}|_{y=\mp L/2} = u_x|_{y=\mp L/2} - U_{\mathrm{wall}}|_{y=\mp L/2}. \tag{59}$$

From Eq. (57), we have

$$u_{\mathrm{slip}}|_{y=\pm L/2} = \frac{gL^2}{2\nu}\left(\mathrm{Kn}+\frac{4}{3}\mathrm{Kn}^2\right) \mp \frac{(U_2-U_1)\mathrm{Kn}}{2\mathrm{Kn}+1}. \tag{60}$$

The slip velocity model is usually characterized by a relation between the slip velocity and the second and the first derivatives of the velocity in the direction normal to the wall. In order to present our results in this form, let us define the reduced $y$ coordinate $\hat{y}=\frac{y}{L}$. Let us also define $\hat{n}$ as the normal of the wall, such that

$$\hat{n}|_{y=\mp L/2} = \pm\hat{y}. \tag{61}$$

With this, we can write the slip velocity as follows:

$$u_{\mathrm{slip}}|_{\mathrm{wall}} = \mathrm{Kn}\left(\frac{\partial u_x}{\partial\hat{n}}\right)_{\mathrm{wall}} - \frac{2}{3}\mathrm{Kn}^2\left(\frac{\partial^2 u_x}{\partial\hat{n}^2}\right)_{\mathrm{wall}}. \tag{62}$$

Note that the results are the same for the top and the bottom walls. The quality of the slip velocity model (62) can be accessed through a comparison with a slip velocity solution

of the Boltzmann-BGK kinetic equation by Cercignani [13]. The result of Cercignani can be written using the notation adopted here as

$$u_{\text{slip}}|_{\text{wall}} = 0.8297\text{Kn}\left(\frac{\partial u_x}{\partial \hat{n}}\right)_{\text{wall}} - 0.5108\text{Kn}^2\left(\frac{\partial^2 u_x}{\partial \hat{n}^2}\right)_{\text{wall}}. \tag{63}$$

It is clear that the result of the D2Q9 model (62) is reasonably close to the full Boltzmann-BGK result (63). In order to make the comparison even more transparent, let us consider the special case of the Poiseuille flow (for simplicity, we set $U_1=U_2=0$). In this case, our solution yields the following slip:

$$u_{\text{slip}}|_{\text{wall}} = \frac{gL^2}{2\nu}\left(\text{Kn} + \frac{4}{3}\text{Kn}^2\right), \tag{64}$$

whereas the result of Cercignani reads

$$u_{\text{slip}}|_{\text{wall}} = \frac{gL^2}{2\nu}(0.8297\text{Kn} + 1.0216\text{Kn}^2). \tag{65}$$

The reduced form of the two results for the slip is compared in Fig. 1.

### C. Flow rate

Another important characteristics of the slip models is the ability to predicting a nonmonotonic dependence of the mass flow rate in the Poiseuille flow on the Knudsen number (so-called Knudsen minimum problem). The flow rate $Q$ is defined as

$$Q = \int_{y=-L/2}^{y=L/2} u_x dy. \tag{66}$$

Assuming Poiseuille flow condition $U_1=U_2=0$ in the general solution (57), and taking into account the relation between the Knudsen number and shear viscosity,

$$\nu = \text{Kn}\frac{c_s L}{\sqrt{3}}, \tag{67}$$

we find the flow rate for the current model as follows:

$$Q = \frac{\sqrt{3}gL^2}{2c_s}\left(\frac{1}{6\text{Kn}} + 1 + \frac{4}{3}\text{Kn}\right). \tag{68}$$

In the continuum limit ($\text{Kn}\to 0$), the solution asymptotically approaches the Navier-Stokes solution,

$$Q_{\text{NS}} = \frac{\sqrt{3}gL^2}{12c_s}\frac{1}{\text{Kn}}. \tag{69}$$

The flow rate (68) has the minimum located at $\text{Kn}_{\text{min}}$, where

$$\frac{1}{\text{Kn}_{\text{min}}} = 2\sqrt{2} \approx 2.828\,43. \tag{70}$$

In the case of Cercignani's slip model, we have

$$Q = \frac{\sqrt{3}gL^2}{2c_s}\left(\frac{1}{6\text{Kn}} + 0.8297 + 1.0216\text{Kn}\right), \tag{71}$$

and the minimum is located at $\text{Kn}_{\text{min}}$, where

$$\frac{1}{\text{Kn}_{\text{min}}} \approx 2.47580. \tag{72}$$

From Fig. 2, it is clear that both the D2Q9 model and the slip-flow approximation based on the Boltzmann-BGK kinetic equation give a reasonably close result for the flow rate.

## VI. HIGHER-ORDER MOMENTS

### A. Shear stress

The shear stress in the present model is purely Newtonian and satisfies a relation

$$P_{xy} = -\rho\nu\frac{\partial u_x}{\partial y}, \tag{73}$$

which can be checked by using Eqs. (57) and (58). However, what is nontrivial is the velocity gradient itself. The Navier-Stokes equation with no-slip boundary condition predicts that the velocity gradient is independent of the Knudsen number. However, we know from the numerical solutions of the linearized Bolztmann equation and DSMC simulations that this is not the case. The present model is able to predict this behavior qualitatively. This agreement is qualitative only due to the absence of kinetic boundary layer (Knudsen layer) in the D2Q9 model [12]. A comparison is possible by introducing a nondimensional velocity gradient $Y$ at the centerline as

$$Y = 1 - \left.(U_2 - U_1)\frac{\partial u_x}{\partial(y/L)}\right|_{y=0}, \tag{74}$$

which can be evaluated for the present model using Eq. (57),

$$Y = \frac{2\text{Kn}}{(2\text{Kn}+1)}. \tag{75}$$

In Table I, the D2Q9 model is compared against data for the linearized Boltzmann-BGK equation [19]. It can be seen from Table I that in the slip-flow regime, the error with respect to the full (not just the slip flow solution) Boltzmann-BGK equation is around 20%, while for the transitional flow it is around 30%. Note that the deviation at higher Knudsen numbers is due to the absence of the Knudsen layer for the velocity in both the D2Q9 model and in the slip flow solution by Cercignani.

### B. Third- and fourth-order moments

From Eq. (34), we have already seen that one of the off-diagonal third-order moments, $Q_{xyy}$, is a function of the longitudinal velocity. That is, the longitudinal energy flux $Q_{xyy}^{\text{neq}}$ reads

$$Q_{xyy}^{\text{neq}} = -2c_s^2\rho g\tau. \tag{76}$$

On the other hand, for the transversal energy flux, we have while using Eq. (30)

TABLE I. Deviation of nondimensional velocity gradient from Navier-Stokes value for the D2Q9 model (75) and the Boltzmann-BGK kinetic equation [19].

| Kn | D2Q9 | Boltzmann-BGK | % Error from Boltzmann-BGK value |
|---|---|---|---|
| 0.06124 | 0.10911 | 0.09134 | 19.45 |
| 0.12247 | 0.19675 | 0.1648 | 19.89 |
| 0.17496 | 0.25922 | 0.2136 | 21.36 |
| 0.24495 | 0.32881 | 0.2664 | 23.43 |
| 0.30619 | 0.37979 | 0.3041 | 24.89 |
| 0.61327 | 0.55051 | 0.4290 | 28.32 |
| 0.81649 | 0.62020 | 0.4821 | 28.64 |
| 1.22474 | 0.71010 | 0.5556 | 27.81 |

$$Q_{yxx}^{\mathrm{neq}} = -\tau \partial_y R_{xxyy}. \tag{77}$$

Furthermore, using Eq. (36),

$$R_{xxyy}^{\mathrm{neq}} = 3c_s^2 \mathcal{N}^{\mathrm{neq}} + \tau(\phi_6 - 3c_s^2 \phi_1), \tag{78}$$

which means that the transversal energy flux is completely determined from the knowledge of the nonequilibrium part of the normal stress difference. Notice that this relationship is equivalent to an algebraic relations offered by Eqs. (35) and (36). In the next section, we shall find the explicit expression for the normal stress difference.

### C. Normal stress difference

Above, we have evaluated the integration constants $k_1$ and $k_2$, which was sufficient to find the velocity and the shear stress in the general unidirectional setup. The remaining two integration constants, $k_3$ and $k_4$, are required in order to find the remaining higher-order moments of the solution. This is the subject of the present section.

Combining Eq. (40) with Eq. (A4), we have

$$X_1(y) = \exp\left(-\frac{\frac{1}{2}+\frac{y}{L}}{\mathrm{Kn}}\right)\{-\rho c_s^2 (u_x^2 - U_1^2)_{y=-L/2} - \Theta_1(y=-L/2)\} + \Theta_1(y),$$

$$X_2(y) = \exp\left(-\frac{\frac{1}{2}-\frac{y}{L}}{\mathrm{Kn}}\right)\{-\rho c_s^2 (u_x^2 - U_2^2)_{y=L/2} - \Theta_2(y=L/2)\} + \Theta_2(y). \tag{79}$$

This general expression can be simplified for special flow situations. In particular, for the Couette flow, we set $g=0$ to get

$$\Theta_1(y) = 2\rho c_s^2 \left(\frac{\mathrm{Kn}^2 (U_2 - U_1)^2}{(2\mathrm{Kn}+1)^2}\right) + 2\sqrt{3} c_s u_x(y) P_{xy},$$

$$\Theta_2(y) = 2\rho c_s^2 \left(\frac{\mathrm{Kn}^2 (U_2 - U_1)^2}{(2\mathrm{Kn}+1)^2}\right) - 2\sqrt{3} c_s u_x(y) P_{xy}. \tag{80}$$

Using Eq. (58) and Eq. (57) in the latter expression, it can be shown that

$$\Theta_1(-L/2) = \rho c_s^2 \left(\frac{\mathrm{Kn}^2 (U_2 - U_1)^2}{(2\mathrm{Kn}+1)^2}\right) - \rho c_s^2 (u_x^2 - U_1^2)_{y=-L/2},$$

$$\Theta_2(L/2) = \rho c_s^2 \left(\frac{\mathrm{Kn}^2 (U_2 - U_1)^2}{(2\mathrm{Kn}+1)^2}\right) - \rho c_s^2 (u_x^2 - U_2^2)_{y=L/2}. \tag{81}$$

Thus,

$$X_1(y) = \rho c_s^2 \left(\frac{\mathrm{Kn}^2 (U_2 - U_1)^2}{(2\mathrm{Kn}+1)^2}\right)\left\{2 - \exp\left(-\frac{\frac{1}{2}+\frac{y}{L}}{\mathrm{Kn}}\right)\right\} + 2\sqrt{3} c_s P_{xy} u_x(y),$$

$$X_2(y) = \rho c_s^2 \left(\frac{\mathrm{Kn}^2 (U_2 - U_1)^2}{(2\mathrm{Kn}+1)^2}\right)\left\{2 - \exp\left(-\frac{\frac{1}{2}-\frac{y}{L}}{\mathrm{Kn}}\right)\right\} - 2\sqrt{3} c_s P_{xy} u_x(y), \tag{82}$$

which is equivalent to the following nonequilibrium normal stress difference:

$$\mathcal{N}^{\mathrm{neq}} = \rho \left(\frac{U_2 - U_1}{L}\right)^2 \frac{\nu^2}{c_s^2 (1+2\mathrm{Kn})^2} \times \left[2 - e^{-1/2\mathrm{Kn}} \cosh\left(\frac{y}{\mathrm{Kn}\, L}\right)\right]. \tag{83}$$

The result (83) was already reported in [12], and we do not dwell on it here. As was explained above, all the remaining higher-order moments are expressed using the nonequilibrium normal stress (83). In particular, the nonequilibrium transversal energy flux $q_y^{\mathrm{neq}} = Q_{yxx}^{\mathrm{neq}}$ reads

$$q_y^{\mathrm{neq}} = Q_{yxx}^{\mathrm{neq}} = \rho \left(\frac{U_2 - U_1}{L}\right)^2 \frac{\sqrt{3}\nu^2}{c_s (1+2\mathrm{Kn})^2} \times \left[e^{-1/2\mathrm{Kn}} \sinh\left(\frac{y}{\mathrm{Kn}\, L}\right) - 2y\right] + P_{xy}(U_1 + U_2). \tag{84}$$

For the pressure-driven flow (Poiseuille flow), the normal stress difference is evaluated in the same way. In this case, combining Eq. (40) with Eq. (A4), we have

$$X_1(y) = \exp\left(-\frac{\frac{1}{2}+\frac{y}{L}}{\mathrm{Kn}}\right)\left\{-\rho g^2 L^2 \left(\frac{3}{4} + 2\mathrm{Kn} + \frac{4}{3}\mathrm{Kn}^2\right) - \Theta_1(y=-L/2)\right\} + \Theta_1(y),$$

$$X_2(y) = \exp\left(-\frac{\frac{1}{2}-\frac{y}{L}}{\mathrm{Kn}}\right)\left\{-\rho g^2 L^2\left(\frac{3}{4}+2\mathrm{Kn}+\frac{4}{3}\mathrm{Kn}^2\right) - \Theta_2(y=L/2)\right\} + \Theta_2(y). \quad (85)$$

Let us now discuss the effect of the choice of the forcing term. For the first type of the forcing, Eqs. (17) and (D1), we have the following relationship:

$$\begin{aligned}\Theta_1(y)+\Theta_2(y) &= \frac{3\rho g^4}{4c_s^4\mathrm{Kn}^2L^2}y^6 + \frac{3\rho g^4}{16c_s^4\mathrm{Kn}^2}(-3-12\mathrm{Kn}+104\mathrm{Kn}^2)y^4 \\ &+ \frac{\rho g^2L^2}{3}(-3-12\mathrm{Kn}+80\mathrm{Kn}^2) \\ &+ \left(16\rho g^2 + \frac{\rho g^4L^2}{64c_s^4\mathrm{Kn}^2}(9+72\mathrm{Kn} \right. \\ &\left. - 192\mathrm{Kn}^2 - 1344\mathrm{Kn}^3 + 15232\mathrm{Kn}^4)\right)y^2 + \frac{\rho g^4L^4}{2304c_s^4\mathrm{Kn}^2} \\ &\times(-27-324\mathrm{Kn}-1080\mathrm{Kn}^2-20340\mathrm{Kn}^4 \\ &- 105984\mathrm{Kn}^5 + 1092608\mathrm{Kn}^6), \end{aligned} \quad (86)$$

$$\begin{aligned}\Theta_1(y)-\Theta_2(y) &= \frac{9\rho g^4}{2c_s^4\mathrm{Kn}L}y^5 + \left(\frac{6\rho g^2}{\mathrm{Kn}L} + \frac{3\rho g^4L}{4c_s^4\mathrm{Kn}}(-3-12\mathrm{Kn}\right. \\ &\left. + 104\mathrm{Kn}^2)\right)y^3 + \left(\frac{3\rho g^2L}{2\mathrm{Kn}}(-1-4\mathrm{Kn}+16\mathrm{Kn}^2)\right. \\ &+ \frac{\rho g^4L^3}{32c_s^4\mathrm{Kn}}(9+72\mathrm{Kn}-192\mathrm{Kn}^2-1344\mathrm{Kn}^3 \\ &\left. + 15232\mathrm{Kn}^4)\right)y. \end{aligned} \quad (87)$$

Therefore,

$$\begin{aligned}\Theta_1(-L/2) = \Theta_2(L/2) &= \rho g^2L^2\mathrm{Kn}\left(4+\frac{40}{3}\mathrm{Kn}\right) \\ &+ \frac{\rho g^4L^4}{36c_s^4}\mathrm{Kn}(27+513\mathrm{Kn}+3456\mathrm{Kn}^2 \\ &+ 8536\mathrm{Kn}^3). \end{aligned} \quad (88)$$

For the second type of forcing [Eqs. (18) and (D2)], we have

$$\begin{aligned}\Theta_1(y) &= 6\rho g^2y^2 + \sqrt{3}c_s\rho gL[2u_x(y)-18\tau g]\left(\frac{y}{L}-\mathrm{Kn}\right) \\ &+ \rho g^2L^2\left[-\left(\frac{y}{L}-\frac{1}{2}\right)\left(\frac{y}{L}+\frac{1}{2}\right)\right. \\ &\left. + \mathrm{Kn} - \frac{2}{3}\mathrm{Kn}^2 + 2\mathrm{Kn}\frac{y}{L}\right], \end{aligned}$$

$$\begin{aligned}\Theta_2(y) &= 6\rho g^2y^2 - \sqrt{3}c_s\rho gL[2u_x(y)-18\tau g]\left(\frac{y}{L}+\mathrm{Kn}\right) \\ &+ \rho g^2L^2\left[-\left(\frac{y}{L}-\frac{1}{2}\right)\left(\frac{y}{L}+\frac{1}{2}\right)\right. \\ &\left. + \mathrm{Kn} - \frac{2}{3}\mathrm{Kn}^2 - 2\mathrm{Kn}\frac{y}{L}\right]. \end{aligned} \quad (89)$$

Therefore,

$$\Theta_1(-L/2) = \Theta_2(L/2) = \rho g^2L^2\mathrm{Kn}\left(4+\frac{40}{3}\mathrm{Kn}\right). \quad (90)$$

As we have already mentioned, both suggestions for the forcing term result in the same expression for the velocity profile, shear stress, and the longitudinal energy flux. The difference occurs only in the higher-order moments such as the normal stress difference. In order to compare the two cases, we introduce the Mach number Ma as the ratio of the average velocity to the speed of sound,

$$\mathrm{Ma} = \frac{u_x^{\mathrm{avg}}}{c_s}, \quad (91)$$

where

$$u_x^{\mathrm{avg}} = \frac{1}{L}\int_{y=-L/2}^{y=L/2} u_x dy = \frac{gL^2}{2\nu}\left(\frac{1}{6}+\mathrm{Kn}+\frac{4}{3}\mathrm{Kn}^2\right). \quad (92)$$

Thus,

$$\mathrm{Ma} = \frac{gL^2}{2\nu c_s}\left(\frac{1}{6}+\mathrm{Kn}+\frac{4}{3}\mathrm{Kn}^2\right). \quad (93)$$

In Figs. 4 and 5, the normal stress difference at the centerline, that is, the maximum of the normal stress difference, is shown as a function of the Knudsen number for two different values of Mach number. From Figs. 4 and 5, we see that both forcing schemes agree with each other at least up to Kn $<0.5$ for low Mach number, as expected. Finally, it should

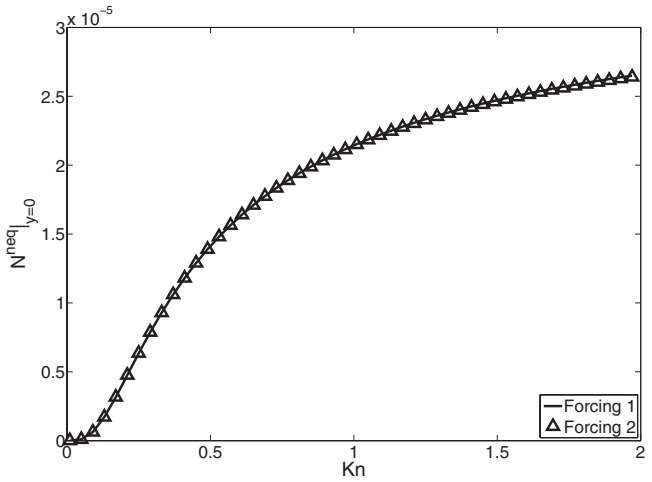


FIG. 4. Comparison of the centerline nonequilibrium normal stress difference ($\mathcal{N}^{\mathrm{neq}}|_{y=0}$) versus Knudsen number at Ma=0.01 for various force terms. Forcing 1: Eq. (17); forcing 2: Eq. (18).

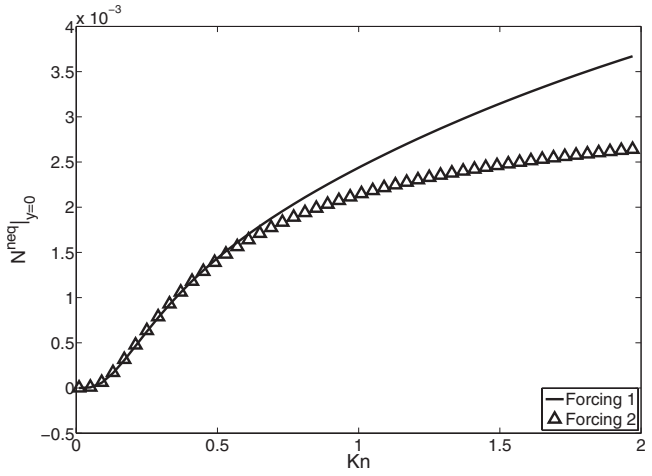


FIG. 5. Comparison of the centerline nonequilibrium normal stress difference ($\mathcal{N}^{neq}|_{y=0}$) versus Knudsen number at Ma=0.1. Notation as in Fig. 4.

be noted that the two forces considered above may show difference in the fully discrete (space and time) LB setting [17]. This, however, goes beyond the focus of our paper.

## VII. DISCUSSION

In this paper, we quantified the standard and very popular lattice Boltzmann model with nine discrete velocities (the D2Q9 model) for the simulation beyond the Navier-Stokes hydrodynamics. The exact solution to the generic unidirectional flow between moving parallel plates extends our result presented in the recent Letter [12]. In particular, we have studied the flow under action of external force. As was already found in [12], the limitation of the D2Q9 model is that it does not describe the Knudsen layer for the velocity profile, and thus the model itself qualifies as a slip-flow approximation. In order to access its quality, we made a comparison with the well-known slip-flow approximation of the Boltzmann-BGK kinetic equation in the Poiseuille flow. The comparison shows that the slip-flow D2Q9 is reasonably close to the slip-flow solution of the Boltzmann-BGK equation. Thus, due to its high computational efficiency, the D2Q9 model can be used for semiquantitative analysis in engineering applications.

It should be remarked that the excellent result is due, not only to the use of the BGK, but also to the choice of the boundary condition. The diffusive wall boundary condition is used, which has been published earlier by two of the present authors [2], and which is only one among many possible choices in the field. It does, however, make sense to use the diffusive boundary condition in this context, because it is derived from the kinetic theory of gases, unlike other commonly used approaches (see, for example, a recent review [20]).

It should be pointed out that our analytic results are pertinent to the discrete-velocity model (15), where time and position variables are continuous. Various discretization procedures for Eq. (15) have already been suggested in the literature; see, for example, [7,21]. Our study thus provides a useful benchmark for various discretization schemes of the kinetic equation (15), and especially for the implementation of the boundary conditions. It has been demonstrated already that, under an appropriate discretization, the numerical solution to the Couette flow converges to the analytical result [12].

We have also analyzed the effect of various force implementations on the higher-order moments and have found that the most popular models of the force agree with each other in a range of Knudsen number for low Mach number flows. Finally, we remind the reader that the D2Q9 model considered in this paper is the lowest-order model in the lattice Boltzmann hierarchy [10] of models. In our followup papers, we shall consider in detail the exact solutions to higher-order isotropic lattice Boltzmann models already announced in [12,22].

## ACKNOWLEDGMENT

I.V.K. gratefully acknowledges support by CCEM-CH. S.A. would like to thank NTU for financial support (Grant No. RG113/06).

## APPENDIX A: POPULATIONS REPRESENTATION IN TERMS OF MOMENTS

From Eq. (44), we can explicitly represent populations $f_i$ in terms of moments,

$$f_0 = \rho - \frac{P_{xx}}{3c_s^2} - \frac{P_{yy}}{3c_s^2} + \frac{R_{xxyy}}{9c_s^4},$$

$$f_1 = \frac{j_x}{2\sqrt{3}c_s} + \frac{P_{xx}}{6c_s^2} - \frac{Q_{xyy}}{6\sqrt{3}c_s^3} - \frac{R_{xxyy}}{18c_s^4},$$

$$f_2 = \frac{j_y}{2\sqrt{3}c_s} + \frac{P_{yy}}{6c_s^2} - \frac{Q_{yxx}}{6\sqrt{3}c_s^3} - \frac{R_{xxyy}}{18c_s^4},$$

$$f_3 = -\frac{j_x}{2\sqrt{3}c_s} + \frac{P_{xx}}{6c_s^2} + \frac{Q_{xyy}}{6\sqrt{3}c_s^3} - \frac{R_{xxyy}}{18c_s^4},$$

$$f_4 = -\frac{j_y}{2\sqrt{3}c_s} + \frac{P_{yy}}{6c_s^2} + \frac{Q_{yxx}}{6\sqrt{3}c_s^3} - \frac{R_{xxyy}}{18c_s^4}$$

$$f_5 = \frac{P_{xy}}{12c_s^2} + \frac{Q_{xyy}}{12\sqrt{3}c_s^3} + \frac{Q_{yxx}}{12\sqrt{3}c_s^3} + \frac{R_{xxyy}}{36c_s^4},$$

$$f_6 = -\frac{P_{xy}}{12c_s^2} - \frac{Q_{xyy}}{12\sqrt{3}c_s^3} + \frac{Q_{yxx}}{12\sqrt{3}c_s^3} + \frac{R_{xxyy}}{36c_s^4},$$

$$f_7 = \frac{P_{xy}}{12c_s^2} - \frac{Q_{xyy}}{12\sqrt{3}c_s^3} - \frac{Q_{yxx}}{12\sqrt{3}c_s^3} + \frac{R_{xxyy}}{36c_s^4},$$

$$f_8 = -\frac{P_{xy}}{12c_s^2} + \frac{Q_{xyy}}{12\sqrt{3}c_s^3} - \frac{Q_{yxx}}{12\sqrt{3}c_s^3} + \frac{R_{xxyy}}{36c_s^4}. \quad \text{(A1)}$$

These expressions can be used to obtain

$$f_5 - f_6 = \frac{P_{xy}}{6c_s^2} + \frac{Q_{xyy}}{6\sqrt{3}c_s^3},$$

$$f_5 + f_6 = \frac{Q_{yxx}}{6\sqrt{3}c_s^3} + \frac{R_{xxyy}}{18c_s^4},$$

$$f_7 + f_8 = -\frac{Q_{yxx}}{6\sqrt{3}c_s^3} + \frac{R_{xxyy}}{18c_s^4},$$

$$f_7 - f_8 = \frac{P_{xy}}{6c_s^2} - \frac{Q_{xyy}}{6\sqrt{3}c_s^3}. \tag{A2}$$

These expressions can be used to write the boundary conditions in terms of the moments. From the boundary condition Eqs. (52) and (53), we have

$$(f_5 + f_6)|_{y=-L/2} = \frac{\rho}{18} + \frac{\rho U_1^2}{18c_s^2},$$

$$(f_7 + f_8)|_{y=L/2} = \frac{\rho}{18} + \frac{\rho U_2^2}{18c_s^2},$$

$$(f_5 - f_6)|_{y=-L/2} = \frac{\rho U_1}{6\sqrt{3}c_s},$$

$$(f_7 - f_8)|_{y=L/2} = -\frac{\rho U_2}{6\sqrt{3}c_s}. \tag{A3}$$

Finally, using Eq. (A2), we get

$$(Q_{xyy} + \sqrt{3}c_s P_{xy})|_{y=-L/2} = \rho c_s^2 U_1,$$

$$(Q_{xyy} - \sqrt{3}c_s P_{xy})|_{y=L/2} = \rho c_s^2 U_2,$$

$$X_1|_{y=-L/2} = \rho c_s^2 (U_1^2 - u_x^2)|_{y=-L/2},$$

$$X_2|_{y=L/2} = \rho c_s^2 (U_2^2 - u_x^2)|_{y=L/2}. \tag{A4}$$

## APPENDIX B: IDENTITIES FOR THE BOUNDARY CONDITION

First, we group the velocity set into three subsets: velocity vectors with positive $y$ velocity, negative $y$ velocity, and zero $y$ velocity. In order to find out contribution to moments by individual subsets, the following identities for the D2Q9 model will be required:

$$\sum_{c_{iy}<0} w_i = \frac{1}{6}, \quad \sum_{c_{iy}<0} w_i c_{ix} = 0, \quad \sum_{c_{iy}<0} w_i c_{iy} = -\frac{1}{6}c,$$

$$\sum_{c_{iy}>0} w_i = \frac{1}{6}, \quad \sum_{c_{iy}>0} w_i c_{ix} = 0, \quad \sum_{c_{iy}>0} w_i c_{iy} = \frac{1}{6}c,$$

$$\sum_{c_{iy}<0} w_i c_{ix}^2 = \frac{1}{18}c^2, \quad \sum_{c_{iy}<0} w_i c_{ix} c_{iy} = 0, \quad \sum_{c_{iy}<0} w_i c_{iy}^2 = \frac{1}{6}c^2,$$

$$\sum_{c_{iy}>0} w_i c_{ix}^2 = \frac{1}{18}c^2, \quad \sum_{c_{iy}>0} w_i c_{ix} c_{iy} = 0, \quad \sum_{c_{iy}>0} w_i c_{iy}^2 = \frac{1}{6}c^2,$$

$$\sum_{c_{iy}<0} w_i c_{ix}^2 c_{iy} = -\frac{1}{18}c^3, \quad \sum_{c_{iy}<0} w_i c_{ix} c_{iy}^2 = 0,$$

$$\sum_{c_{iy}<0} w_i c_{ix}^2 c_{iy}^2 = \frac{1}{18}c^4,$$

$$\sum_{c_{iy}>0} w_i c_{ix}^2 c_{iy} = \frac{1}{18}c^3, \quad \sum_{c_{iy}>0} w_i c_{ix} c_{iy}^2 = 0,$$

$$\sum_{c_{iy}>0} w_i c_{ix}^2 c_{iy}^2 = \frac{1}{18}c^4, \tag{B1}$$

where $c = \sqrt{3}c_s$.

## APPENDIX C: DERIVATION OF THE RESULT OF DISTRIBUTION FUNCTION SUMMATION FOR FLUID CONFINED BETWEEN PARALLEL PLATES

First of all, we calculate

$$\sum_{\mathbf{c}_i\cdot\mathbf{n}<0} w_i \left(\rho + \frac{j_\alpha c_{i\alpha}}{c_s^2}\right) = \sum_{\mathbf{c}_i\cdot\mathbf{n}<0} w_i \left(\rho + \frac{j_x c_{ix}}{c_s^2} + \frac{j_y c_{iy}}{c_s^2}\right) = \frac{\rho}{6} + 0 + 0 = \frac{\rho}{6}, \tag{C1}$$

since $\Sigma_{\mathbf{c}_i\cdot\mathbf{n}<0} w_i c_{ix} = 0$ and $j_y = 0$.

Next, term by term, by applying the identities from Eq. (B1), we have

$$\begin{aligned}\sum_{\mathbf{c}_i\cdot\mathbf{n}<0} w_i \left(\frac{\mathcal{G}_i^{(2)}}{2c_s^4}\right) &= \frac{1}{2c_s^4} \sum_{\mathbf{c}_i\cdot\mathbf{n}<0} w_i \big[(P_{xx} - \rho c_s^2)(c_{ix}^2 - c_s^2) \\ &\quad + (P_{yy} - \rho c_s^2)(c_{iy}^2 - c_s^2) + 2P_{xy} c_{ix} c_{iy}\big] \\ &= \frac{1}{2c_s^4}\left[(P_{xx} - \rho c_s^2)\left(\frac{1}{18}3c_s^2 - \frac{1}{6}c_s^2\right)\right. \\ &\quad \left. + (\rho c_s^2 - \rho c_s^2)\left(\frac{1}{6}3c_s^2 - \frac{1}{6}c_s^2\right) + 0\right] = 0,\end{aligned} \tag{C2}$$

$$\begin{aligned}\sum_{\mathbf{c}_i\cdot\mathbf{n}<0} w_i \left[\frac{\mathcal{G}_i^{(3)}}{6c_s^6}\right] &= \frac{1}{6c_s^6} \sum_{\mathbf{c}_i\cdot\mathbf{n}<0} w_i \big[3(Q_{yxx} - j_y c_s^2)(c_{ix}^2 c_{iy} - c_{iy} c_s^2) \\ &\quad + 3(Q_{xyy} - j_x c_s^2)(c_{ix} c_{iy}^2 - c_{ix} c_s^2)\big] \\ &= \frac{1}{2c_s^6}\left[(Q_{yxx} - j_y c_s^2)\left(\mp\frac{1}{18}c^3 - \mp\frac{1}{6}c c_s^2\right)\right. \\ &\quad \left. + (Q_{xyy} - j_x c_s^2)(0 - 0)\right] \\ &= \frac{1}{2c_s^6}\left[(Q_{yxx} - j_y c_s^2)\left(\mp\frac{1}{18}3c_s^2 - \mp\frac{1}{6}c_s^2\right)c\right.\end{aligned}$$

$$+ (Q_{xyy} - j_x c_s^2)(0-0) \Bigg] = 0, \tag{C3}$$

$$\begin{aligned}
\sum_{\mathbf{c}_i\cdot\mathbf{n}<0} w_i \left[\frac{\mathcal{G}_i^{(4)}}{4c_s^8}\right] &= \frac{1}{4c_s^8} \sum_{\mathbf{c}_i\cdot\mathbf{n}<0} w_i (R_{xxyy} - P c_s^2 + \rho c_s^4) \\
&\quad \times (c_{ix}^2 - c_s^2)(c_{iy}^2 - c_s^2) \\
&= \frac{1}{4c_s^8} \sum_{\mathbf{c}_i\cdot\mathbf{n}<0} w_i (R_{xxyy} - P c_s^2 + \rho c_s^4) \\
&\quad \times [c_{ix}^2 c_{iy}^2 - (c_{ix}^2 + c_{iy}^2) c_s^2 + c_s^4] \\
&= \frac{1}{4c_s^8} (R_{xxyy} - P c_s^2 + \rho c_s^4) \\
&\quad \times \left[\frac{1}{18} c^4 - \left(\frac{1}{18} c^2 + \frac{1}{6} c^2\right) c_s^2 + \frac{1}{6} c_s^4\right] \\
&= \frac{1}{4c_s^8} (R_{xxyy} - P c_s^2 + \rho c_s^4) \\
&\quad \times \left[\frac{1}{18} 9 c_s^4 - \left(\frac{4}{18} 3 c_s^2\right) c_s^2 + \frac{1}{6} c_s^4\right] = 0,
\end{aligned} \tag{C4}$$

which complete the proof.

## APPENDIX D: MOMENTS OF FORCINGS

For the first type of forcing, Eq. (17), we have

$$\begin{aligned}
\phi_1(\mathcal{F}^{(1)}) &= \left(2j_x - \frac{j_x^3}{\rho^2 c_s^2}\right) g_x, \\
\phi_2(\mathcal{F}^{(1)}) &= j_y g_x + j_x g_y, \\
\phi_3(\mathcal{F}^{(1)}) &= \left(2j_y - \frac{j_y^3}{\rho^2 c_s^2}\right) g_x \\
\phi_4(\mathcal{F}^{(1)}) &= j_y \left(\frac{2j_x}{\rho} - \frac{j_x^3}{\rho^3 c_s^2}\right) g_x + \left[\frac{j_x^2}{\rho}\left(1 - \frac{j_y^2}{\rho^2 c_s^2}\right) + \rho c_s^2\right] g_y, \\
\phi_5(\mathcal{F}^{(1)}) &= \left[\frac{j_y^2}{\rho}\left(1 - \frac{j_x^2}{\rho^2 c_s^2}\right) + \rho c_s^2\right] g_x + j_x \left(\frac{2j_y}{\rho} - \frac{j_y^3}{\rho^3 c_s^2}\right) g_y, \\
\phi_6(\mathcal{F}^{(1)}) &= \left(2c_s^2 - \frac{j^2}{\rho^2}\right)(j_x g_x + j_y g_y) + 3 j_x g_x \frac{j_y^2}{\rho^2} + 3 j_y g_y \frac{j_x^2}{\rho^2}.
\end{aligned} \tag{D1}$$

For the second type of forcing, Eq. (18), we have

$$\begin{aligned}
\phi_1(\mathcal{F}^{(2)}) &= 2 j_x g_x, \\
\phi_2(\mathcal{F}^{(2)}) &= j_y g_x + j_x g_y, \\
\phi_3(\mathcal{F}^{(2)}) &= 2 j_y g_y, \\
\phi_4(\mathcal{F}^{(2)}) &= \rho c_s^2 g_y, \\
\phi_5(\mathcal{F}^{(2)}) &= \rho c_s^2 g_x, \\
\phi_6(\mathcal{F}^{(2)}) &= 2 c_s^2 (j_x g_x + j_y g_y).
\end{aligned} \tag{D2}$$


[1] A. Beskok and G. E. Karniadakis, *Microflows: Fundamentals and Simulation* (Springer, Berlin, 2001).
[2] S. Ansumali and I. V. Karlin, Phys. Rev. E **66**, 026311 (2002).
[3] S. Succi, Phys. Rev. Lett. **89**, 064502 (2002).
[4] B. Li and D. Kwok, Phys. Rev. Lett. **90**, 124502 (2003).
[5] X. D. Niu, C. Shu, and Y. Chew, Europhys. Lett. **67**, 600 (2004).
[6] S. Ansumali and I. V. Karlin, Phys. Rev. Lett. **95**, 260605 (2005).
[7] V. Sofonea and R. Sekerka, J. Comput. Phys. **207**, 639 (2005).
[8] J. Horbach and S. Succi, Phys. Rev. Lett. **96**, 224503 (2006).
[9] S. Ansumali, I. V. Karlin, and H. C. Öttinger, Europhys. Lett. **63**, 798 (2003).
[10] S. S. Chikatamarla and I. V. Karlin, Phys. Rev. Lett. **97**, 190601 (2006).
[11] A. N. Gorban and I. V. Karlin, *Invariant Manifolds for Physical and Chemical Kinetics* (Springer, Berlin, 2005).
[12] S. Ansumali, I. V. Karlin, S. Arcidiacono, A. Abbas, and N. Prasianakis, Phys. Rev. Lett. **98**, 124502 (2007).
[13] C. Cercignani, *Theory and Application of the Boltzmann Equation* (Scottish Academic Press, Edinburgh, 1975).
[14] I. V. Karlin, A. Ferrante, and H. C. Öttinger, Europhys. Lett. **47**, 182 (1999).
[15] Y. H. Qian, D. d'Humieres, and P. Lallemand, Europhys. Lett. **17**, 479 (1992).
[16] X. He, X. Shan, and G. Doolen, Phys. Rev. E **57**, R13 (1998).
[17] Z. Guo, C. Zheng, and B. Shi, Phys. Rev. E **65**, 046308 (2002).
[18] D. d'Humiéres, Prog. Astronaut. Aeronaut. **59**, 450 (1992).
[19] D. R. Willis, Phys. Fluids **5**, 127 (1962).
[20] I. Ginzburg, F. Verhaeghe, and D. d'Humiéres, Comm. Comp. Phys. **3**, 427 (2008).
[21] X. He, S. Chen, and G. D. Doolen, J. Comput. Phys. **146**, 282 (1998).
[22] I. V. Karlin and S. Ansumali, Phys. Rev. E **76**, 025701(R) (2007).